THE SOFT X-RAY TELESCOPE FOR THE SOLAR-A MISSION*

S. TSUNETA

Institute of Astronomy, University of Tokyo, Mitaka, Tokyo 181, Japan

L. ACTON, M. BRUNER, J. LEMEN, W. BROWN, R. CARAVALHO, R. CATURA, S. FREELAND, B. JURCEVICH, M. MORRISON

Lockheed Palo Alto Research Laboratory, Palo Alto, CA 94304, U.S.A.

Y. OGAWARA

Institute of Space and Astronomical Sciences, Sagamihara, Japan

T. HIRAYAMA

National Astronomical Observatory of Japan, Mitaka, Tokyo 181, Japan

and

J. OWENS

Marshall Space Flight Center, Huntsville, AL 35812, U.S.A.

Abstract. The Soft X-ray Telescope (SXT) of the SOLAR-A mission is designed to produce X-ray movies of flares with excellent angular and time resolution as well as full-disk X-ray images for general studies. A selection of thin metal filters provide a measure of temperature discrimination and aid in obtaining the wide dynamic range required for solar observing. The co-aligned SXT aspect telescope will yield optical images for aspect reference, white-light flare and sunspot studies, and, possibly, helioseismology. This paper describes the capabilities and characteristics of the SXT for scientific observing.

1. Introduction

The Soft X-ray Telescope (SXT) will provide, for the first time, the opportunity to image the Sun in X-rays over a long period of time with both high temporal and spatial resolution. It gives SOLAR-A an important capability for solar science beyond the study of flares, the primary objective of the mission. The SXT instrument was jointly developed by the Lockheed Palo Alto Research Laboratory and the National Astronomical Observatory of Japan. Collaborators include the University of Tokyo, Stanford University, the University of California at Berkeley, and the University of Hawaii.

The SXT instrument that makes the observations in support of our scientific objectives is a glancing incidence telescope of 1.54 m focal length which forms X-ray images in the 0.25 to 4.0 keV range on a 1024 × 1024 virtual phase charge coupled device (CCD) detector. A selection of thin metallic filters located near the focal plane provides the capability to separate different X-ray energies for plasma temperature diagnostics.

* After the launch the name of SOLAR-A has been changed to YOHKOH.

Solar Physics **136:** 37–67, 1991.

Knowledge of the location of X-ray images with respect to features observable in visible light is provided by a coaxially mounted visible-light telescope which forms its image on the CCD detector when the thin metallic filter is replaced by an appropriate glass filter.

The ability of the instrument to perform its observational tasks to the levels necessary to achieve our objectives is highly dependent on the optical performance of the X-ray mirror and the quality of the CCD detector. Other determining factors are the stability of the metering structure and the quality of the instrument calibration. Finally, versatility of instrument control and discriminating utilization of limited telemetry are key to the success of the experiment.

1.1. Scientific objectives

Soft X-ray images reveal the distribution of high-temperature coronal gas and, thus, the structure of the confining magnetic field and thus the topological context of solar activity. SOLAR-A will, for the first time, provide simultaneous soft and hard X-ray images with good angular and temporal resolution. The SXT X-ray images will be searched for the following kinds of information:

- The geometry of the X-ray emitting structures and the inferred coronal magnetic field topology;
- the temperature and density of X-ray emitting plasma;
- the spatial and temporal characteristics of flare energy deposition;
- the transport of energetic particles and conduction fronts;
- the presence of waves or other magnetic field disturbances associated with sprays, filament eruptions, and coronal transients; and
- the locations of energy release and particle acceleration.

The SXT will, by itself, contribute new insights into solar physics. Yet, many studies will benefit from study of correlated observations made with all the SOLAR-A instruments and simultaneous observations made with ground-based solar radio and optical telescopes. Concrete steps have been taken (e.g., Morrison *et al.*, 1991) to facilitate joint analysis of different types of solar observations. The primary objective of the SOLAR-A mission is flare research. SXT will contribute to answering the questions of the following type:

- Are there observable pre-flare conditions which give rise to an energetic flare?
- Are there observable discriminators between flares with strong nonthermal effects, e.g., high-energy particle acceleration and mass ejection, and those that exhibit primarily thermal properties?
- Is flare energy released continuously or in discrete pulses (elementary flares)?
- What is the filling factor of coronal and flare loops?
- What is the characteristic time for the acceleration process?
- Are electrons and ions accelerated simultaneously by the same process? Are there multiple phases or steps in the acceleration process to cover the wide range of energy (non-relativistic to relativistic) and mass (electrons, protons, and heavier ions)?
- Are there observational clues to the location and dimensions of the acceleration

region? Might it be spatially coincident with the location of hard X-ray and gamma-ray emission?

– How is the energy, generated during a flare, redistributed during evolution through different flare phases?

– Is it possible to observe or infer how and where the energetic particles propagate from the acceleration region? Do they diffuse or propagate in well-collimated beams?

– What is the relationship between the energetic particles which escape from the Sun into the interplanetary space and those which remain at the Sun and produce hard X-ray, gamma-ray, radio, and other emissions?

In addition to the objectives for flare studies the SXT will provide a powerful instrument for non-flare coronal physics. Regular full-disk coronal images will be acquired for the purpose of study of the evolution of the magnetic morphology of the Sun's corona. We hope to elucidate better the appearance, migration, and reconnection of magnetic flux over time scales of a few minutes to a few years by following the creation, change and disappearance of coronal X-ray structures. Studies of the appearance and evolution of coronal magnetic holes will contribute to both solar and solar system physics. We are interested to observe systematically X-ray bright points and clarify their role in the appearance (or disappearance) of magnetic flux. Careful cinematographic studies of the X-ray corona, along with coordinated observations of the visible layers below, may provide new clues to the nature of coronal heating.

The SXT visible-light aspect telescope will provide, in addition to its primary use for precise X-ray/visible alignment information, cinematographic observations of white-light flares and sunspots. Furthermore, a possibility exists to use it for helioseismological studies. It is estimated that intensity oscillations as small as $dI/I \approx 10^{-7}$ may be detected if the SXT data stream is dedicated to this experiment for several months (Sakurai, 1990).

1.2. SXT INSTRUMENT REQUIREMENTS

The SXT has been designed to provide the following capabilities:

– A dynamic range of $> 10^7$ to cover the expected brightness range;

– time resolution of 2 s or better to cover the evolution of the impulsive phase;

– angular resolution of ≤ 3 arc sec to lcoate flare footpoints and observe the filling of loop structures;

– a field-of-view large enough to image the whole solar disk;

– a spectral diagnostic capability sufficient to estimate plasma temperature;

– the capability to record images in visible light, co-aligned with the soft X-ray images, for study of relationships of X-ray and white-light flares and to enable precise registration with other solar data;

– ability to withstand a severe launch environment (20 g r.m.s. vibration levels);

– fundamental mechanical resonance frequency above 100 MHz; and

– the SXT must operate over a temperature range of 0 to +25 °C.

2. Optics

In concept, the SXT is a very simple instrument. It has a fixed focus and comprises a sensor, a shutter, dual filter wheels and two co-aligned imaging elements, a mirror for X-rays and a lens for visible light. The position of the filter wheels determine whether an X-ray or an optical picture is taken. There is a commandable door behind the lens, not shown in Figure 1 for clarity, used to exclude visible light from the telescope when desired.

The mechanical and optical design of the SXT required maintaining focus and alignment through a difficult launch and thermal environment with low mass, power,

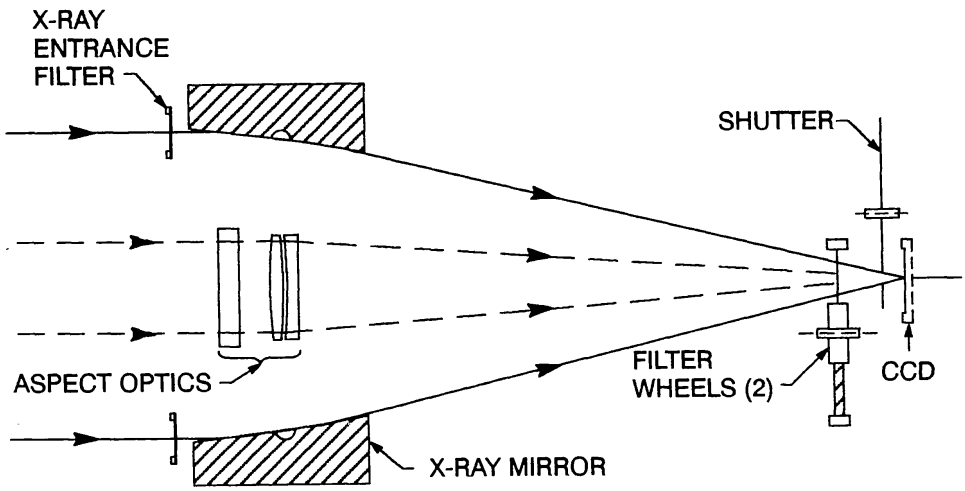

Fig. 1a. Schematic illustration of the optical concept and key elements of the SXT.

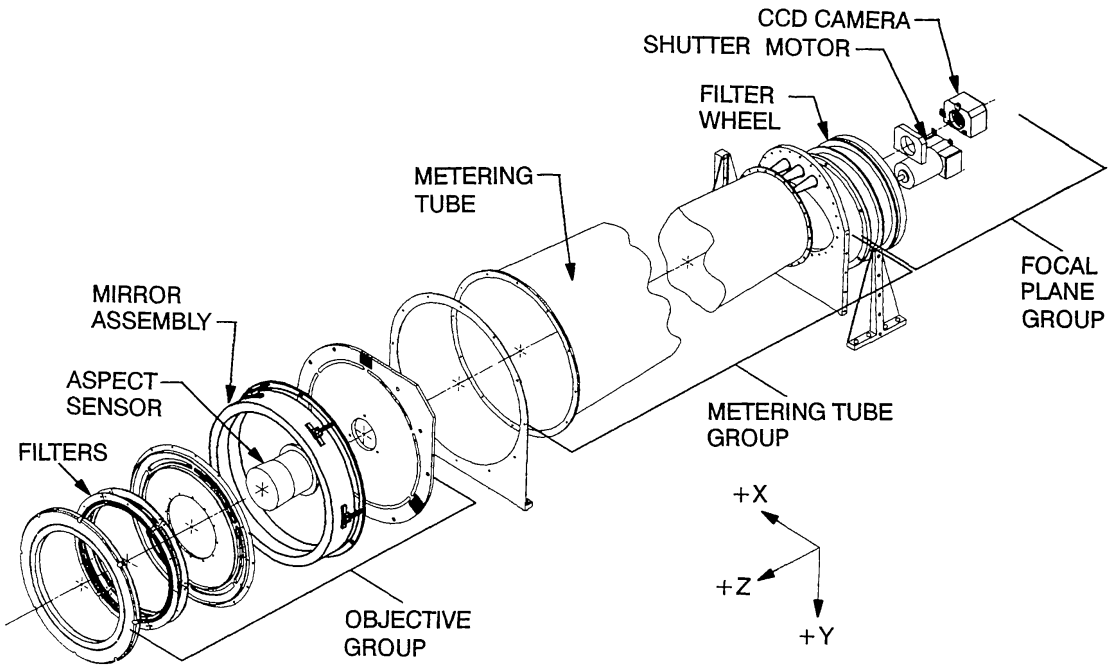

Fig. 1b. Exploded diagram of the SXT. Sub-assemblies mentioned in the text are identified.

and dollar budgets. The technical solution to these challenges has been described by Bruner *et al.* (1989). The description of SXT in this paper will be limited to that useful for understanding the scientific performance of the instrument. Although the calibration and characterization of SXT given here is preliminary, it is mature enough for confident use in predicting SXT performance and for first-order data interpretation.

2.1. Overall SXT response

Characteristics of the SXT are presented in Table I. The composite spectral sensitivity of the basic telescope is illustrated in Figure 2(a). Figures 2(b–e) show how this sensitivity is modified by the X-ray analysis filters. These filters have been carefully designed to optimize the ability to determine solar plasma temperature (Section 2.5). The variation of the effective area of the SXT as a function of off-axis angle is illustrated in Figure 3.

The same CCD detector (Section 2.4) is used for X-ray and visible-light images. The metallic X-ray analysis filters or a commandable door block the visible light from the aspect telescope aperture so that it does not contaminate the X-ray images. The angular pixel size of the CCD (2.45″) is approximately the same as the angular resolution of both the X-ray and aspect telescopes. The CCD subtends 42 × 42 min of arc and so furnishes full-disk and coronal coverage in a single image. SXT provides for commandable on-chip pixel summation in order to increase the field of view for the same time resolution. The angular resolution in each summation mode is 1 × 1 (2.45″), 2 × 2 (4.9″), and 4 × 4 (9.8″). The image data are normally compressed and decompressed from 12 to 8 for telemetry and back to 12 bits on the ground for analysis through the use of look-up tables based on a square-root algorithm (Section 3).

Both aspect and X-ray exposures are controlled by a rotating mechanical shutter driven by a constant velocity motor. The shutter blade has two sector openings, one of 3 deg and one of 60 deg. For the very shortest exposure (1 ms) the narrow sector is driven past the CCD without pause. Three such passes in quick succession provide a 3 ms exposure while driving the 60 deg sector past provides a nominal 20 ms exposure. For longer exposures the 60 deg sector is used and the shutter blade stops in the open position for a prescribed period of time. The exposure duration is measured on board by a hardware timer. The shutter is used in combination with a 8.05% transmission metal mesh in the filter wheel to obtain the effective exposures listed in Table II. Note that the exposure error and non-uniformity do not add algebraically. For example, total uncertainty for command 0 will be about 3.0%.

2.2. X-ray telescope

Within the SXT, the X-rays are brought to a focus by a glancing incidence mirror of unique technology. This optic utilizes hyperboloids of revolution for both optical surfaces (Nariai, 1987, 1988) to achieve better wide-field angular resolution on a flat focal plane than would the familiar paraboloid-hyperboloid design. Wide-field performance is further enhanced by making the mirror unusually short (4.5 cm total) along the optical axis (Watanabe, 1987). Both optical surfaces of the mirror are formed in a single cylinder

TABLE I

SXT characteristics

General	
Weight	
telescope	14.7 kg
electronics	9.0 kg
Average daytime power	7–12 W, plus heaters
Envelope	30 × 30 × 170 cm
Control	On-board computers
CCD detector (operated cooled to −18 °C)	
Array size	1024 × 1024
Pixel size	18.281 ± 0.002 μm = 2.4528 ± 0.0005″
On-chip summation	2 × 2 and 4 × 4
Digital signal	12 bit compressed to 8 bit
Time resolution	0.5 s (special mode)
64 × 64 pixel image	2.0 s (normal)
X-ray telescope	
Diameter	230.65 mm
Geometrical area	261.75 mm^2
Peak effective area	78 mm^2 at 8 Å
Effective focal length	1535.6 mm
Spectral range	3–45 Å at 1% of peak response
Resolution	≤3″ FWHM over solar disk at 8 Å
Plate scale	134.2″ mm^{-1}
Dynamic range	$> 5 \times 10^9$
Aspect telescope	
Aperture	50 mm
Effective focal length	1538.4 ± 0.5 mm
Transmission	0.013% from 3500 to 4500 Å
Filter wheels	

Commanded position	Front wheel	Rear wheel
1	Open	Open
2	30 Å at 4310 Å	Al 1265 Å
3	CCD flood lens	Al/Mg/Mn composite
4	Opal-glass diffuser	Be 119 μm
5	140 Å at 4580 Å	Al 11.6 μm
6	8.05% mesh	Mg 2.52 μm

Rotating sector shutter	
Effective exposure range	0.077 ms–242 s
Number of steps	37

of low-expansion Zerodur glass-ceramic which is bonded into a lightweight titanium stress-free mount. The reflecting surfaces are covered with an evaporated coating of 420 Å of gold on top of 80 Å of chromium. For wavelengths longer than 6 Å where scattering is moderate the agreement between predicted and calibrated mirror effective area agree to better than 90%. Further description of this optic and its calibration is published separately (Lemen *et al.*, 1989, 1991).

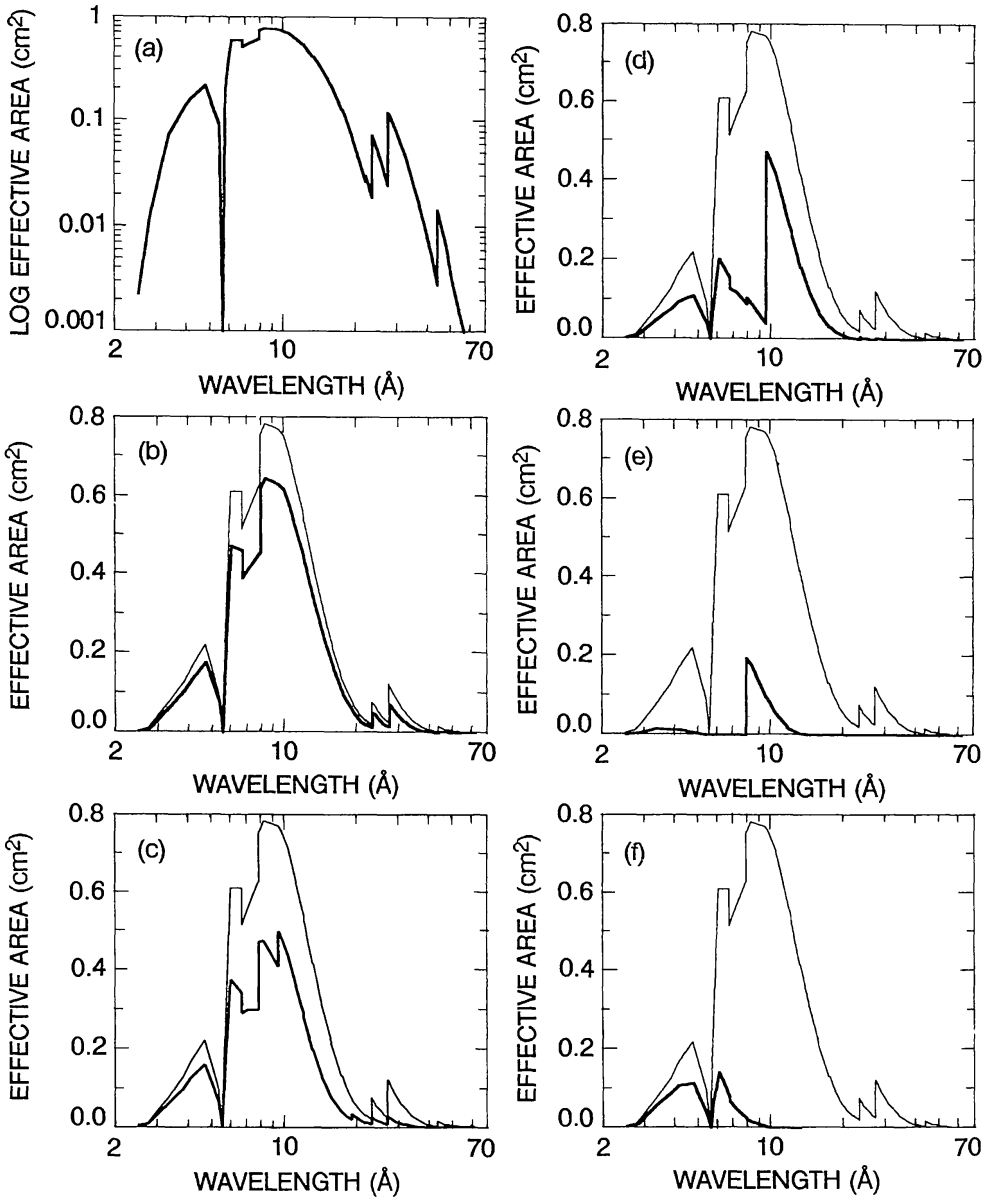

Fig. 2. Effective area of the SXT: (a) no analysis filter, (b) 1265 Å Al filter, (c) composite filter comprising 2930 Å Al, 2070 Å Mg, 562 Å Mn, and 190 Å C, (d) 2.52 μm Mg, (e) 11.6 μm Al, and (f) 119 μm Be. (b)–(f) compare the no-filter case (light line) with the filtered case (heavy line). (a) is plotted on a logarithmic scale to better illustrate regions of small effective area, which may dominate SXT response when the solar spectrum is intense at those wavelengths.

Glancing incidence X-ray mirrors are often troubled by broad, intense, scattering haloes. This is especally troublesome for solar flare observing where scene contrast over small angular scales is extreme and, at the same time, scientifically important. This small angle scattering is dominated by surface roughness and mid-frequency errors of figure. For SXT, a surface roughness of 3.8 Å r.m.s. and mid-frequency error of 51 Å r.m.s. was achieved. The point spread profile of the telescope, acquired with a flight-type CCD, is illustrated in Figure 4.

The angular resolving power of an under-sampled X-ray telescope like SXT is not

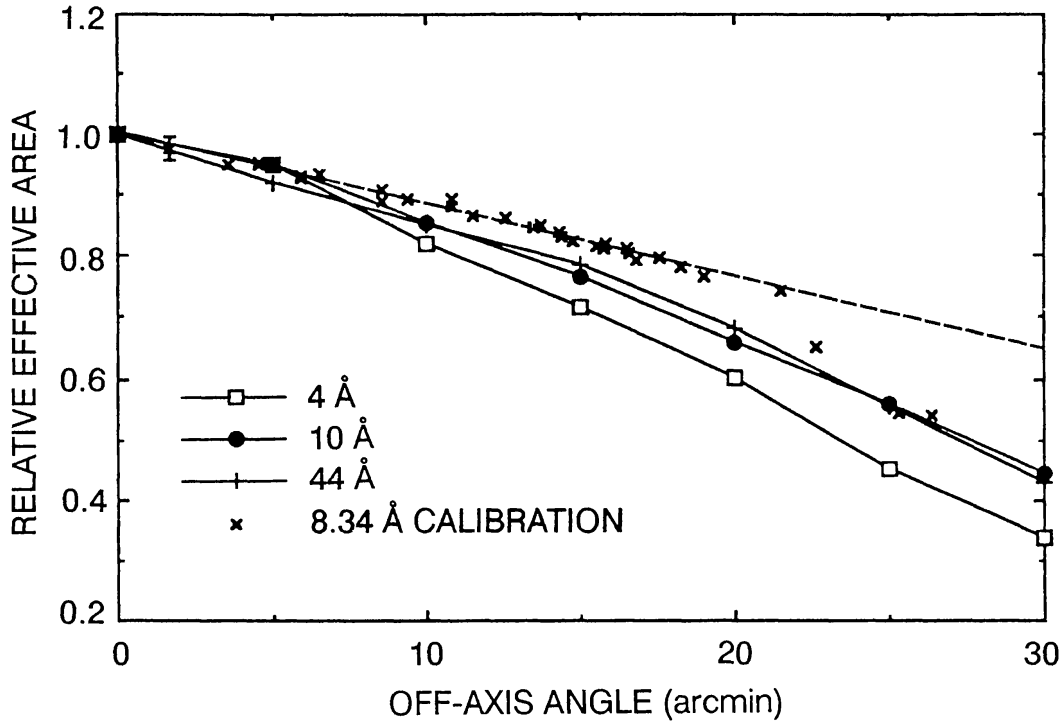

Fig. 3. Variation of effective area of SXT with off-axis angle determined by ray tracing (without X-ray scattering) for three different wavelengths. Calibration data at 8.34 Å are shown with a straight line fit to the calibration results inside of 23 arc min.

easy to characterize in simple terms. The X-ray point spread function (PSF) of the instrument is defined as the empirical expression that describes the intensity distribution over the image of a point source at infinity. The PSF is a function of wavelength and off-axis angle. One figure of merit useful for X-ray mirrors is the diameter, D_{50}, of the circle that encloses 50% of the imaged energy. For SXT, calibration data yields the following expression for this parameter (on-axis) over the 4–45 Å interval:

$$D_{50} = 7.0 - 2.4 \log_{10} \lambda \text{ arc sec}\,, \tag{1}$$

where λ is the wavelength in Å.

A second common means of characterizing the PSF is the full width at one-half maximum (FWHM) of the best fitting 2-dimensional Gaussian (Figure 5). Quantitatively, this is a poor choice for comparing telescopes because the intrinsic PSF has a very sharp central spike (Lemen *et al.*, 1989). For such a PSF the FWHM is sensor-dependent because the definition of maximum reflects pixel size down to very small pixels (or film grain). Also, the wings of the profile are distinctly non-Gaussian. A modified Moffat PSF (Bendinelli, 1991) has been found to fairly accurately characterize the PSF of the SXT. The form of this expression is

$$N = \frac{C}{\left[1 + \left(\frac{r}{a}\right)^2\right]^b}\,, \tag{2}$$

TABLE II

SXT effective exposures

Command	Effective exposure	Error (%)	Non-uniformity (%)
0	0.077 ms[a]	1.4	2.6
1	0.23 ms[a]	1.4	2.6
2	0.96 ms	1.4	2.6
3	1.38 ms[a]	1.4	2.3
4	2.88 ms	1.4	2.6
5	3.08 ms[a]	1.3	≤0.1
6	4.69 ms[a]	0.8	≤0.1
7	6.30 ms[a]	0.6	≤0.1
8	9.50 ms[a]	0.4	≤0.1
9	17.2 ms	1.4	2.3
10	28.8 ms	3.2	1.0
11	38.2 ms	1.3	≤0.1
12	58.3 ms	0.8	≤0.1
13	78.3 ms	0.6	≤0.1
14	118 ms	0.4	≤0.1
15	168 ms	≤0.4	≤0.1
16	238 ms	≤0.4	≤0.1
17	338 ms	≤0.4	≤0.1
18	468 ms	≤0.4	≤0.1
19	668 ms	≤0.4	≤0.1
20	948 ms	≤0.4	≤0.1
21	1.34 s	≤0.4	≤0.1
22	1.89 s	≤0.4	≤0.1
23	2.67 s	≤0.4	≤0.1
24	3.78 s	≤0.4	≤0.1
25	5.34 s	≤0.4	≤0.1
26	7.55 s	≤0.4	≤0.1
27	10.7 s	≤0.4	≤0.1
28	15.1 s	≤0.4	≤0.1
29	21.4 s	≤0.4	≤0.1
30	30.2 s	≤0.4	≤0.1
31	42.7 s	≤0.4	≤0.1
32	60.4 s	≤0.4	≤0.1
33	85.4 s	≤0.4	≤0.1
34	121 s	≤0.4	≤0.1
35	171 s	≤0.4	≤0.1
36	242 s	≤0.4	≤0.1

[a] The 8.05% transmission mask is applied.

where N is the signal in a pixel in digital data numbers (DN), C, a, and b are parameters of the fit, and r is the radial coordinate of the function, expressed in pixels.

The SXT is equipped with two entrance filters in series for the purpose of excluding visible and UV light from the telescope. The filters comprise Lexan as the support material, Al for thermal control and to exclude visible light, and Ti to exclude the intense solar He 304 Å emission. The dual filter design was chosen to minimize the possibility of stray light entering the instrument through a pinhole in the metal films.

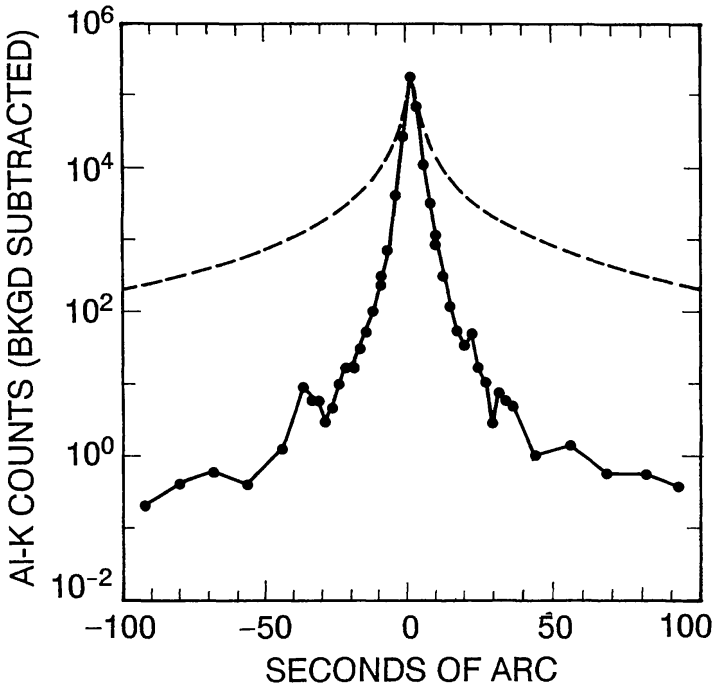

Fig. 4. Measured point spread profile of SXT at 8.34 Å (Al K line) for 1″ source at 310 m. Equivalent curve for Skylab SO-54 telescope (Vaiana *et al.*, 1977) is shown as a dashed line for comparison. Great improvement in decreased scattering wings for SXT is evident.

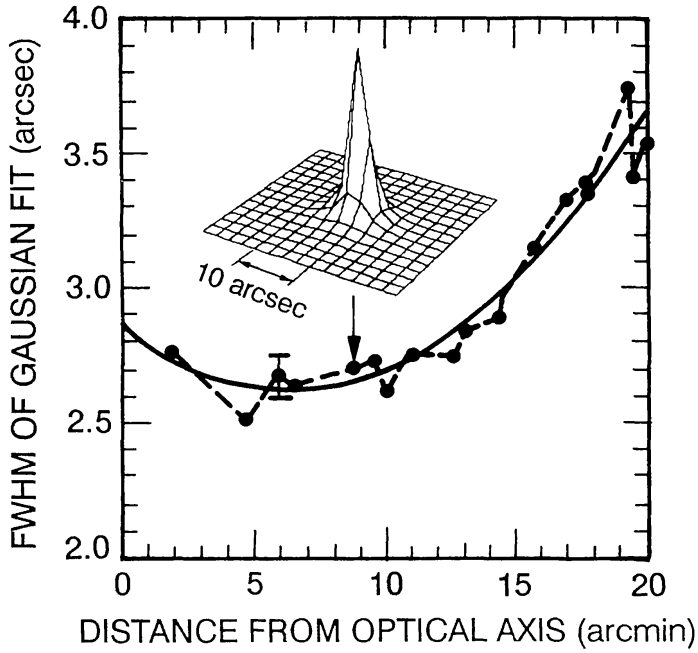

Fig. 5. Approximate FWHM of the SXT image of a point source versus distance from optical axis. The vertical scale is seconds of arc with an estimated uncertainty of about 10%. The inset shows the surface plot of the image at the point indicated by the arrow. A typical 1σ error bar is shown. A parabola has been fitted through the points. The CCD has been deliberately placed 0.1 mm ahead of the position of best on-axis focus in order to achieve a more uniform resolution across the solar disk.

The 5 X-ray analysis filters of the SXT, located in the rear filter wheel, are designed to provide attenuation, increasing the dynamic range of the instrument, and a measure of flare temperature information (Section 2.5). Four of the filters are supported on stainless steel mesh. Figure 2 illustrates the response of the SXT through the various filters. The 8.05% transmission stainless steel mesh located in the front filter wheel can be used in tandem with any of the positions of the rear wheel to extend the dynamic range of the instrument. Analysis of calibration images has not revealed any measurable effect on images taken with this attenuating mesh.

2.3. Aspect Telescope

The SXT aspect sensor is a high-quality, albeit small, optical telescope in its own right. It serves several purposes:

(1) Sunspot and limb images for determining SXT pointing to an accuracy of 1 sec of arc or better and to aid image registration with ground-based data.

(2) To record magnetic plage, sunspot and pore motions and development in and around active regions.

(3) To observe white-light flares.

(4) For helioseismology.

(5) To provide flat field illumination for CCD gain calibration.

(6) To provide a source of blue light for photon flood of the CCD for the purpose of annealing soft X-ray degradation of the sensor.

The objective lens assembly forms an image of the same scale as the X-ray image that is co-aligned to approximately one pixel. The actual co-alignment will be verified in orbit by overlay of the white-light limb with the X-ray absorption limb using full-disk images. The assembly allows just enough light into the SXT to acquire properly exposed aspect pictures in about 0.1 s.

The entrance filter consists of a white-light attenuator and a bandpass filter. The white-light attenuator is composed of a synthetic fused silica substrate with a 500 Å aluminum attenuating layer, under a dielectric coating for durability, on the rear surface. The bandpass filter is deposited on a 6 mm thick substrate of Hoya CM-500 blue glass. The transmission of the white-light attenuator and the bandpass filter in tandem is illustrated in Figure 6. The combined out of band rejection of the white-light attenuator and bandpass filter is of order 10^{-8}.

The image of the aspect telescope is formed by a doublet lens, which is achromatic across the entrance filter's passband. The lens has a 50 mm clear aperture and a focal length of 1538 mm, forming a beam which is approximately $f/31$. The doublet has a depth of focus of approximately ± 0.5 mm, with an Airy disk diameter of about 50 microns. Lenses have been selected to give the best match to the measured effective focal length of the SXT X-ray mirror. Optical materials for the objective lens assembly have been selected, by specification or test, for their radiation resistance. All appropriate surfaces have been anti-reflection coated.

The SXT filter wheel carries two optical band pass filters. Magnetic plage in and around active regions will be readily visible in the 30 Å filter centered on the CN band

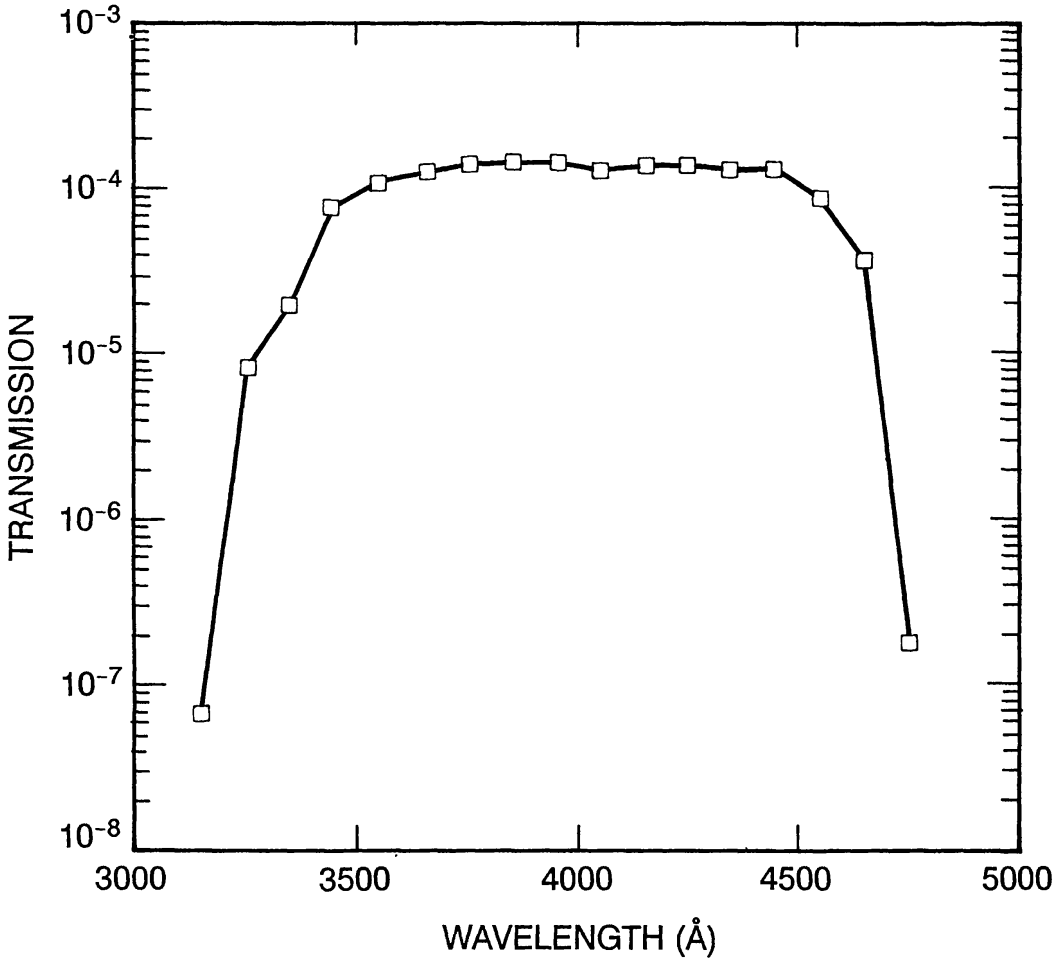

Fig. 6. Spectral transmission of the objective lens assembly.

at 4308 Å. In order to acquire a continuum image with a filter that is less subject to drift over the life of the mission we have also included a 140 Å filter centered at about 4580 Å. These filters are equipped with neutral density attenuators on the rear side to balance the exposure times and to attenuate ghosts from back reflections off of the CCD to less than 1%. The bandpasses of these two filters are illustrated in Figure 7.

2.4. CCD IMAGE SENSOR

The CCD camera for the SXT utilizes a 1024 × 1024 virtual phase CCD (VPCCD) with 18.3 μm pixels, manufactured specifically for SXT by Texas Instruments at their Miho, Japan, facility. The principal of operation of the VPCCD has been described by Hynecek (1979) and Janesick, Hynecek, and Blouke (1981). Virtual phase technology is a good choice for SXT because the thin oxide layer covering the virtual well provides excellent soft X-ray response without the difficulties of thinned, back illuminated, operation.

The SXT camera is operated in a charge-collection, rather than a photon counting, mode. Solar features are typically bright enough to produce near full well images with exposures of less than 1 s. Because of the high signal levels, SXT requirements on read

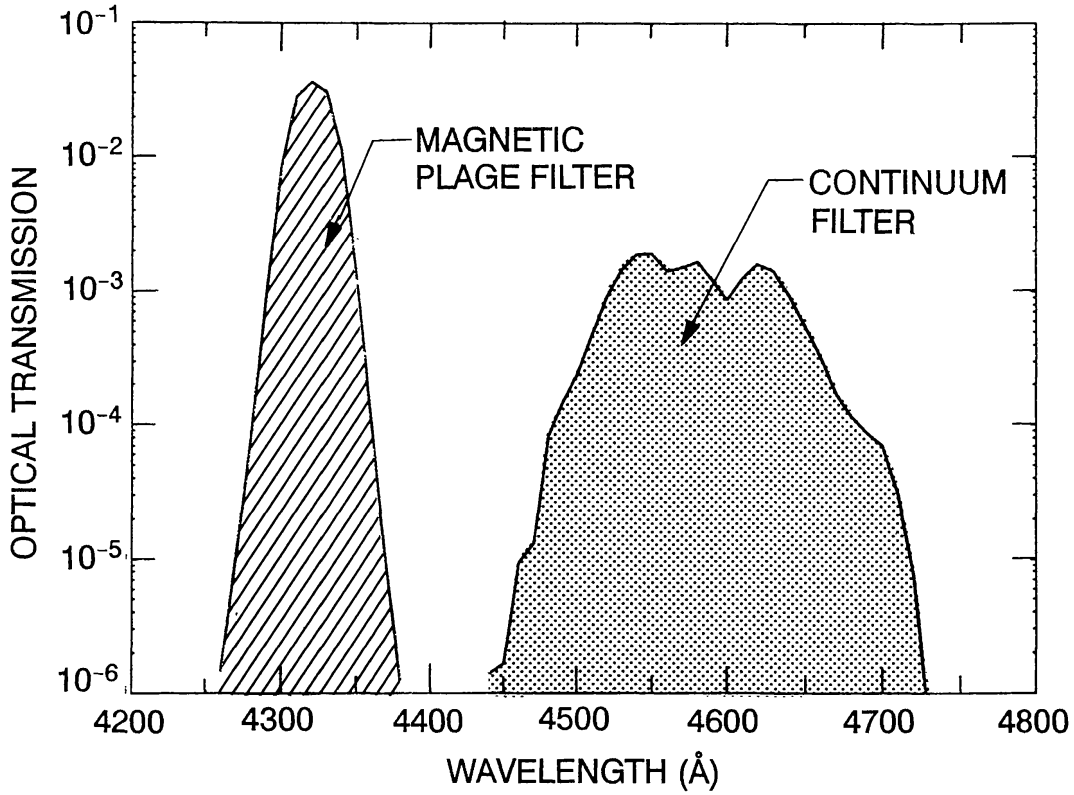

Fig. 7. Spectral transmission of the aspect telescope bandpass filters.

noise and dark current are not stringent. Dark-current control and gain stability are obtained by cooling the CCD to -18 °C with a closed-loop 3-stage thermoelectric cooler. CCD read noise is about 85 electrons pixel^{-1} r.m.s. Average dark current at -18 °C is about 9 electrons pixel^{-1} s^{-1} (0.4 picoamp cm^{-2}). Charge transfer efficiency of the SXT flight sensor measured 0.999989 for signals $> 10^4$ electrons. The forward filter wheel includes an opal glass diffuser to provide flat field illumination of the CCD for the purpose of gain calibration through use of the photon transfer curve technique (Janesick, Klaasen, and Elliott, 1987). Figure 8 shows the pixel structure and the measured quantum efficiency of the SXT flight device. The quantum efficiency of the CCD for blue light from the aspect sensor is roughly 30%.

The full well capacity of the CCD is about 250 000 electrons. At the conversion constant of 3.65 eV electron^{-1} for Si this results in a full well capacity of about $10^3 \times 1$ keV (12.4 Å) photons. Extensive use of 2×2 and 4×4 on-chip summing is anticipated so the camera gain has been set low (100 electrons per digital number (DN)) to preclude excessive saturation of the 12 bit analog to digital convertor. For full-resolution observations (no on-chip summation) the CCD will saturate before the 12-bit ADC attains full scale in order to assure that maximum CCD signal capacity is available. For summed exposures the ADC will saturate first. Managing to achieve correct exposures, especially on flares, will be challenging. This task will normally be assigned to the on-board automatic exposure control described below. The CCD

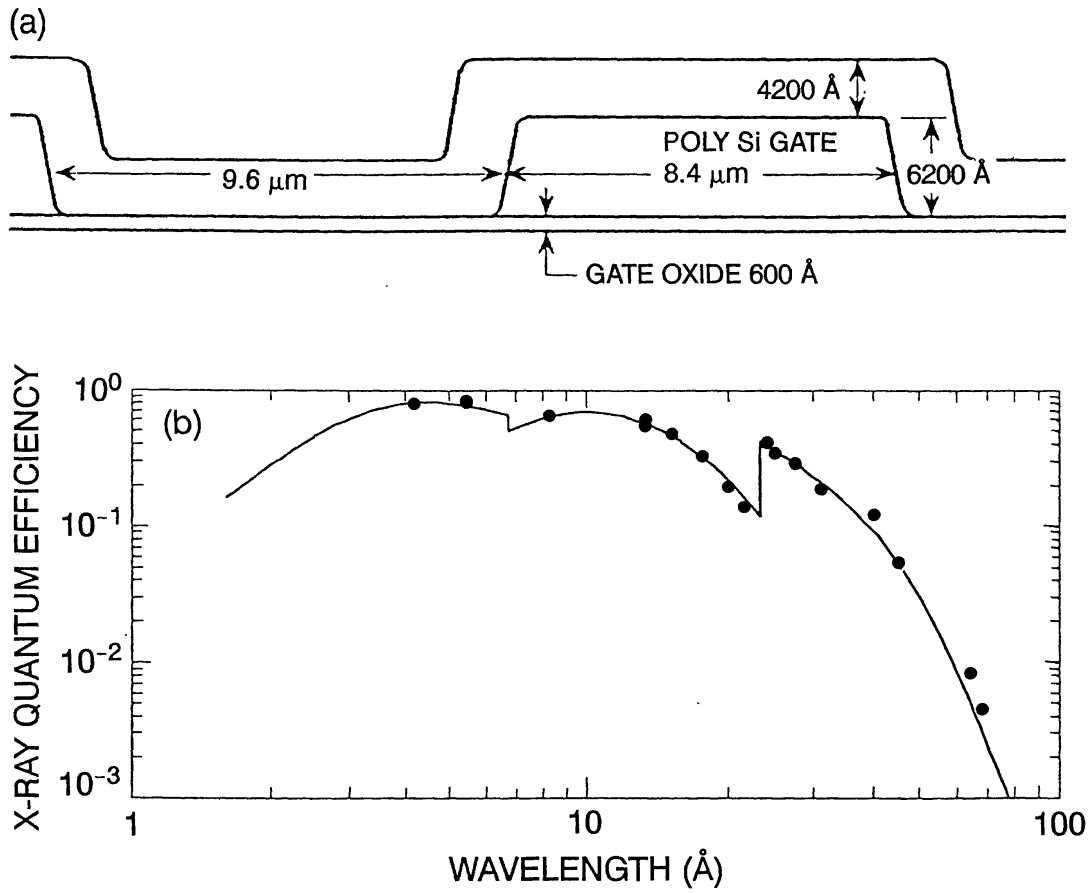

Fig. 8. (a) Pixel structure of CCD from electron microscopy. (b) Solid curve shows the computed quantum efficiency (QE) of the CCD calculated from the measured pixel structure. The points are QE calibration data obtained at Lockheed for the SXT flight device. Statistical error of these data is smaller than the plotted points.

camera can also be operated in a pseudo-frame transfer mode in the event of problems with the mechanical shutter.

The SXT CCD is subject to degradation from cosmic rays, energetic protons trapped in the Earth's radiation belts and from the solar X-rays themselves. These problems have been treated in detail for SXT by Acton *et al.* (1991). Because the sensor is operated cooled and exposures are normally a fraction of a second, the increased dark current and dark spikes (pixels with greatly enhanced dark current) produced by energetic particles do not appear to pose a significant threat to SXT science over the 3–5 year mission lifetime. However, ionization produced in the thin oxide layer of the CCD by the solar X-rays produces increased dark current and, eventually, loss of charge transfer efficiency with resulting smearing of the solar images. It has been discovered that illumination of the CCD with blue light from the aspect telescope apparently creates free electrons at the Si–SiO_2 interface, neutralizing the charge and annealing the damage. The SXT filter wheel has been equipped with a slightly negative quartz lens for the purpose of flooding the entire CCD with 3300–4700 Å light. The duration of this photon flood can be set by command. Present plans call for doing such a flood for approximately the first 4 min of each daylight pass, while the spacecraft's attitude is stabilizing.

2.5. SXT RESPONSE TO THE SUN

The SXT is capable of imaging solar plasma over the temperature range of < 1 to > 50 MK for a wide range of intensities. The sensitivity of the SXT for detecting solar features of different temperatures is illustrated in Figure 9. These curves are produced

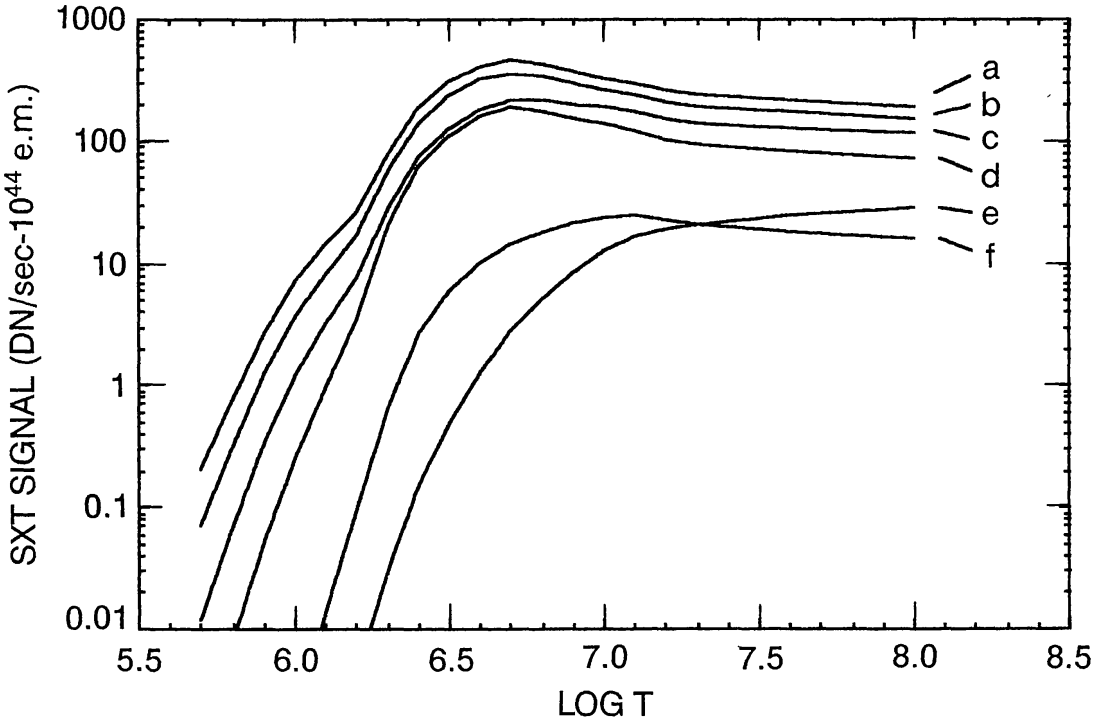

Fig. 9. Total signal as a function of $\log_{10} T$ for the open filter case (a) and the SXT analysis filters: (b) Al 1265 Å, (c) Al/Mg/Mn, (d) Mg 2.52 μm, (e) Al 11.6 μm, (f) Be 119 μm.

by convolving the instrument response functions of Figure 2 with the theoretical X-ray emission line spectra of Mewe, Gronenschild, and van den Oord (1985) and the continuum expression of Mewe, Lemen, and van den Oord (1986). Note that these curves assume an emission measure of 10^{-44} cm^{-3}. In thinking of SXT sensitivity it is important to keep in mind that, even for a point source, only about half of the CCD signal will appear in the brightest pixel.

Because the solar soft X-ray spectrum is predominantly a line spectrum, the well-defined absorption edges (Figure 2) of the SXT analysis filters emphasize detection of certain spectral lines or groups of lines. This provides rudimentary spectral, and hence temperature, discrimination. Figure 10 presents the ratio of signals versus $\log_{10} T$ for selected pairs of analysis filters. The two thickest filters will, in general, not work for non-flare temperatures because of inadequate sensitivity. Similarly, the open telescope (no analysis filter) and thinnest filters may saturate in flares, even for the shortest exposures. For isothermal sources the uncertainty in plasma temperature determined by this technique is of about 0.1 in $\log_{10} T$.

In principle, the response curves of Figure 9 can be treated in the same way as the emissivity curves for an atomic emission line for differential emission measure (DEM)

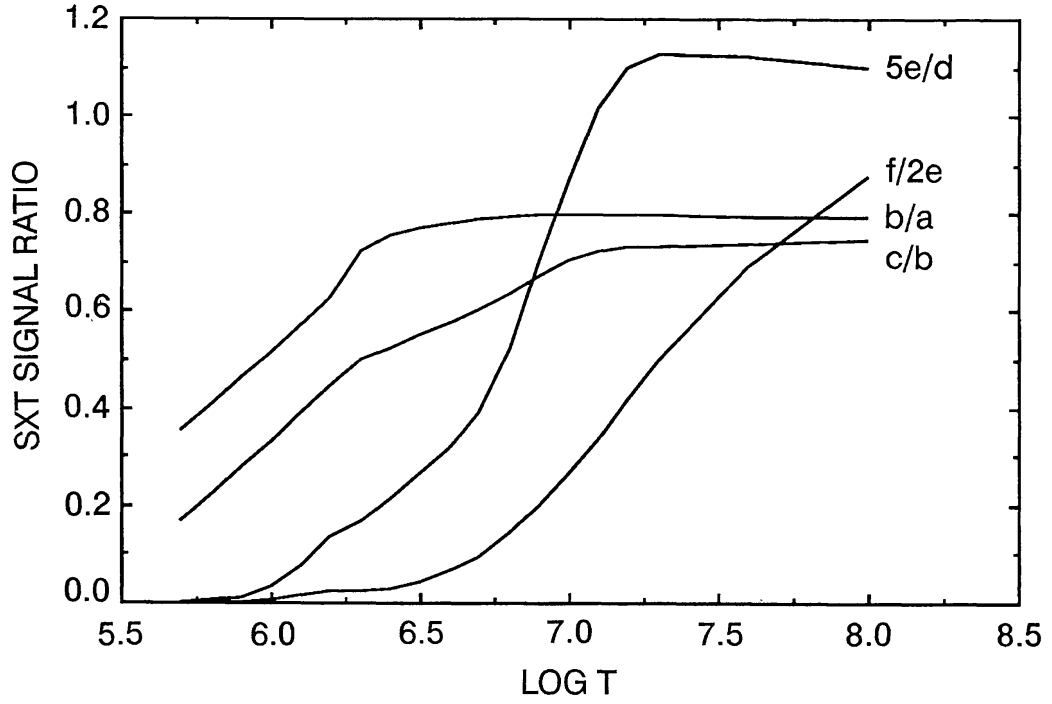

Fig. 10. Ratios of the SXT response functions of Figure 9. In 2 cases, 5e/d and f/2e, observing time with e, the 11.6 μm Al filter, must be increased by factors of 5 and 2, respectively, with respect to the other filter to achieve the given ratio.

analysis of a multi-thermal plasma. In practice, the problem is more ill-conditioned (Craig and Brown, 1986) than the atomic line case. Figure 11 illustrates the results of a simulation of such an analysis. Here, SXT signals were predicted for the given DEM and put through a version of the Sylwester analysis program (Fludra and Sylwester, 1986) to generate a DEM (Strong *et al.*, 1991). This work indicates that the DEM reliably reflects the presence of high-temperature plasma and the total emission measure is well determined. However, detailed structure or peaks in the DEM distribution are not reproduced and the low-temperature end is poorly determined in the presence of Poisson counting statistics.

Photon statistics will contribute the dominant error in SXT photometry. A CCD signal of 100 electrons produced an increment of one digital number (DN) from the ADC. At 3.65 eV electron^{-1}, this corresponds to detecting a single photon of wavelength 34 Å. The 1σ readout and detector noise on a typical image will be roughly 1 DN. The true photon statistics in a thin-filter image will be additionally uncertain because of the factor of 10 range in photon energies to which the SXT is sensitive. Thicker filters restrict the spectral acceptance band of the instrument so that the statistical error can be more accurately estimated.

Table III demonstrates the predicted signal from a single SXT pixel through each of the SXT analysis filters for a variety of solar features (Strong and Lemen, 1987) and exposures appropriate for their observation. The angular extent of typical features is taken into account. McTiernen (1991) has examined the response of the SXT to two non-thermal (power-law spectrum) events which were partially occulted by the Sun from

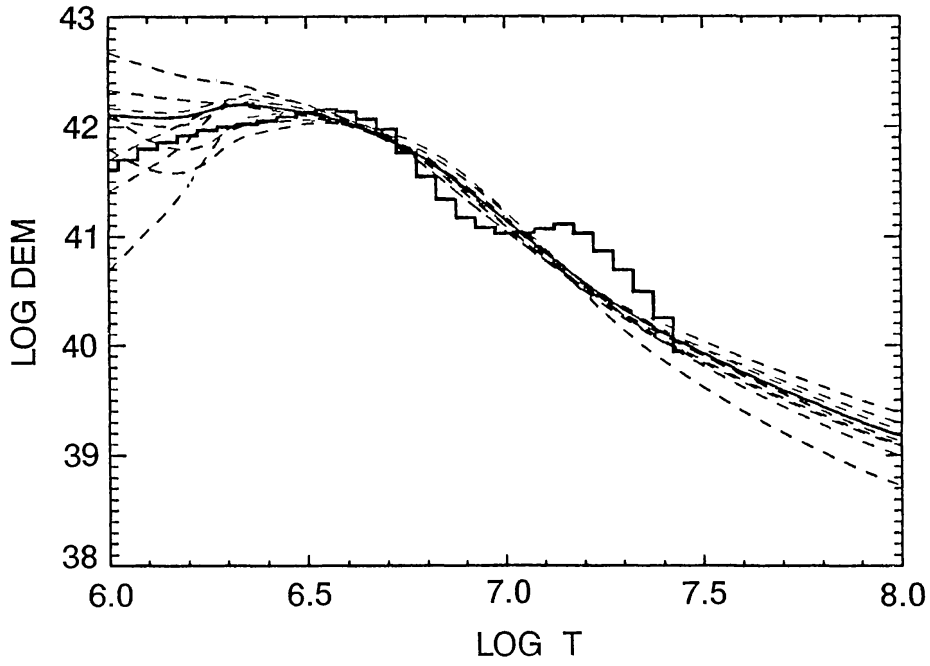

Fig. 11. Results of a simulated derivation of a differential emission measure distribution (DEM) using SXT images through all 6 analysis filters (Strong *et al.*, 1991). The histogram is the input distribution. The solid curve is the best-fit model derived from the input data. The dashed curves represent additional random solutions reflecting Poisson counting statistics.

the ISEE-3/ICE spacecraft (Kane *et al.*, 1979). He estimated that the flare of 16 February, 1984, which was visible beyond 160 000 km above the surface of the Sun and exhibited a photon power-law spectral index of about 4.6, would have generated a signal of 500–1500 DN pixel^{-1} s^{-1} in the SXT with no filter. Such sources in the high corona above the limb should be observable by SXT. The spectral index of the emission can be found using thick/thin filter ratios. For this flare the uncertainty in the spectral index using a ratio of the thick beryllium filter to the thin aluminum filter would be approximately 0.6, although the SXT alone could not distinguish between power law and thermal spectra.

3. SXT Image Data

The acquisition of solar images by the SXT is controlled by electornics and software operating within the SOLAR-A Data Processor (DP). This function is slaved in frequency to the SOLAR-A telemetry rate. Images will normally be taken under either high (32 kbps) or medium (4 kbps) rate. Low rate (1 kbps) is used only for night mode. In the discussion to follow, examples of image frequency will always assume high-rate telemetry unless otherwise noted. For medium rate operation, picture frequency decreases by a factor of eight.

The CCD camera employs a 12-bit ADC but data are transferred to the DP as 8-bit numbers. For purposes of gain calibration and helioseismology it is important to maintain the full 12-bit accuracy. This is accomplished by transferring either the high-

1991SoPh..136...37T

TABLE III

Examples of SXT response

Feature	Temp. (MK)	Em. meas. (cm^{-3})	Exposure (s)	Open	Al 1265	Al/Mg/Mn	Mg 2.5	Al 11.6	Be 119
				Signal (DN) in one pixel					
Coronal hole	1.3	2E+42	60.4	18	10	4	1	0	0
X-ray bright point	1.8	7E+43	0.948	34	23	11	6	0	0
Large-scale loops	2.1	6E+42	5.34	30	22	11	8	0	0
Active region	2.5	3E+45	0.468	sat.	2034	1064	878	37	2
Long duration event (LDE)	7.5	1E+48	0.00096	sat.	sat.	1958	1515	201	74
Impulsive C flare	12	5E+48	0.00023	sat.	sat.	2047	1449	286	180
M flare	17	2E+48	0.00023	1191	938	690	464	101	92
X flare	20	1E+49	0.000077	1886	1501	1101	723	162	163
Post-flare loop	7	3E+46	0.0172	2084	1671	1070	856	104	344

order or low-order 8 bits, selectable by command. Normally, the ADC numbers are compressed to 8 bits according to the following algorithm. Taking, N, X, and M to be the original, compressed and decompressed digital numbers, respectively,

– for $N \leq 64$:

$$X(N) = N\,, \qquad M = X = N\,; \tag{3}$$

– for $N > 64$:

$$\begin{aligned} X(N) &= \text{round}\,(59.249 + \sqrt{3510.39 - 9.50(431.14 - \mathrm{N})}\,), \\ M &= \text{round}\,(0.10526X^2 - 12.473X + 431.14)\,, \quad (X < 255)\,, \\ M &= 4085\,, \qquad\qquad\qquad\qquad\quad (X = 255)\,, \end{aligned} \tag{4}$$

where N is the CCD camera output (Digital Number or DN), X is the 8-bit compressed number, M is the 12-bit decompressed value.

Ignoring read noise, dark current, and spurious charge, which are on the order of 1 DN, the data number is given by

$$N = \frac{nhv}{3.65c} + 11.5\,, \tag{5}$$

where n = number of photons detected, hv = mean photon energy in eV, c = CCD camera gain constant of 100 electrons DN^{-1}; 11.5 is a digital offset in the CCD camera.

This yields the relation

$$n = \frac{(N - 11.5)\lambda}{34}\,, \tag{6}$$

and correspondingly

$$m = \frac{(M - 11.5)\lambda}{34}\,, \tag{7}$$

where λ is the photon wavelength in Å.

Finally, the compression error may be expressed in terms of photon statistics as

$$\varepsilon = \sqrt{\frac{\lambda}{34}}\,\frac{N - M}{\sqrt{N - 11.5}}\,. \tag{8}$$

3.1. Image formats

Images from the CCD camera of the SXT are transferred to image buffers in the SOLAR-A Data Processor (DP) for processing and read out to telemetry. There are three types of pictures, Full Frame Images (FFI), Partial Frame Images (PFI) and patrol images. In the following discussion a 'line of CCD data' will include 1024 × 1, 1024 × 2, or 1024 × 4 actual CCD pixels and be 1024, 512, or 256 output pixels long depending

on whether 1 × 1, 2 × 2, or 4 × 4 on-chip summation is used. The FFI comprise 512, 256, 128, or 64 lines of CCD data so that at highest resolution (i.e., no on-chip pixel summation) they are, at most, only one half of a CCD picture. For on-chip summation modes, however, full CCD pictures can be taken. For PFI 64 lines of CCD data are always transferred to the buffer but, normally, only a subset of these data are sent to telemetry. In our terminology a PFI is a 64 × 64 sub-image that will include 64 × 64, 128 × 128, or 256 × 256 actual CCD pixels, depending upon the use of on-chip summation. For both FFI and PFI the band of CCD lines transferred to the DP is referred to as a Region of Interest (ROI). Patrol images are always 128 lines of CCD data acquired with 4 × 4 pixel summation (one-half of a CCD picture). Patrol images are used in the DP for Automatic Observing Region Selection (ARS). The patrol images are not normaly sent to telemetry.

For FFI the entire content of the image buffer is always sent to telemetry, i.e., is read out to the 10 Mbyte Bubble Data Recorder or transmitted directly to ground in real time. From the contents of the PFI buffer up to 16 adjacent (in the E–W direction) 64 × 64 pixel PFI are extracted from the 64 line image strips and sent to telemetry. Finally contiguous assemblies of PFI of any rectangular shape from a single PFI on up are called Observing Regions (OR). Four different shapes of observing regions are illustrated in Figure 12.

The arrangement and size of an X-ray or optical solar image on the CCD of the SXT

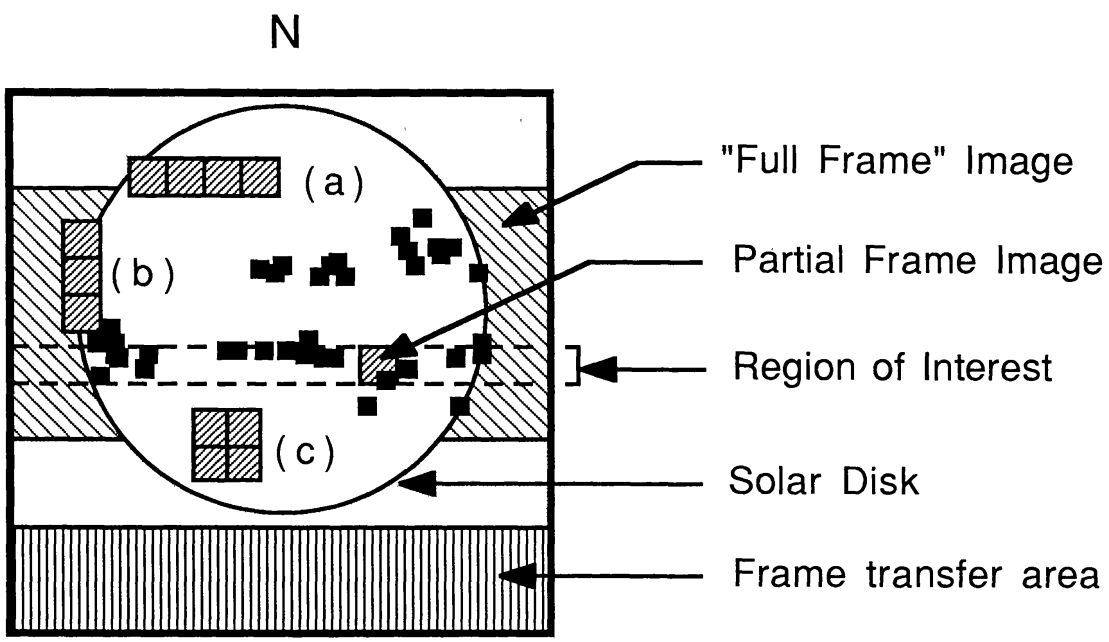

Fig. 12. Arrangement of a solar image on the CCD. Ecliptic north is up and the solar west limb is to the left. Locations of 43 large flares observed by SMM in 1980 are indicated by black squares. The 'full frame' image comprises the largest number of pixels that can be sent to telemetry as an individual image. More typically, a partial frame image comprising 64 × 64 pixels, extracted from a designated region of interest, is sent to telemetry. In order to increase the size of an observing region the partial frame images may be grouped as illustrated by (a), (b), and (c). Observing regions of type (a) can be imaged with a single exposure whereas (c) requires 2 exposures and (b) requires 3 individual exposures. These examples are the size obtained when on-chip pixel summation is not used, i.e., at best angular resolution.

is shown in Figure 12. The vertical or column direction of the CCD is oriented towards ecliptic north. The solar image is deliberately de-centered upwards on the sensor to provide an unilluminated area at the bottom of the CCD. This area may serve as a frame transfer register to permit shutterless operation of the instrument in the event of trouble with the rotating mechanical shutter. In the frame transfer mode the portion of the picture to be saved would be rapidly shifted down into the frame transfer and then read into the image buffer at the normal rate of 131 072 pixels s^{-1}.

Considerable flexibility has been introduced into schemes of SXT image acquisition in order to make optimum use of the telemetry capacity of SOLAR-A. First, on-chip 2×2 and 4×4 pixel summation can be used to trade resolution for data rate. Second, the full frame images of 64, 128, 256, or 512 lines can be taken anywhere on the CCD to observe solar active longitudes of interest. Third, the region of interest of the partial frame images can be taken anywhere on the CCD and the 64×64 PFIs may be grouped together into larger Observing Regions (OR) as illustrated by examples (a), (b), and (c) of Figure 12. Observing regions of type (a) which are only extended E–W are acquired in a single exposure. Each block in the N–S direction, such as in examples (b) and (c), require a separate exposure. Although ORs with multiple-PFI extent N–S are assembled on the ground, they are treated as a single entity in planning and commanding. The angular extent of an FFI and a single PFI for the 3 summation modes are given in Table V.

3.2. Experiment Control

SXT operation is under the control of software running in the SOLAR-A data processor (DP) computer and the SXT microprocessor. It is the function of the DP to command the SXT and to receive, format, and transfer all data to telemetry. It is the function of the SXT microprocessor to control the SXT mechanisms and CCD camera as directed by the DP. Command and status information is exchanged between the two computers via a block of memory in the SXT microprocessor which serves as a 'mailbox'.

The DP has the capability to examine SXT image data to select regions of interest and to adjust the length of the SXT exposure. It also monitors data from the hard X-ray, soft X-ray, or Bragg crystal spectrometers and may issue a flare flag to initiate SOLAR-A flare mode.

3.2.1. *Sequence Tables*

At the most fundamental level, the following parameters must be specified for each SXT exposure:

- Location and size of portion of CCD image to be sent to telemetry;
- on-chip CCD pixel summation of 1×1, 2×2, or 4×4;
- exposure duration;
- filter(s) to be used.

In addition, there are secondary instrument functions which may need to be altered and parameters that must be set (in all about 20 items).

The setup of the SXT for each observation is accomplished from tables of parameters

stored in the DP called sequence tables. Each table provides all of the information necessary to define an SXT observing sequence, which can be quite complex. These tables, in turn, address other tables of fixed or adjustable control parameters. A sequence table is organized as a set of nested 'do-loops' in which a sequence of commands is executed repetitively until the prescribed number of cycles has been completed, at which time the program continues on to the next task.

This structure is illustrated in Table IV along with an example of an observing sequence for study of the evolution of a medium-sized active region. The sequence starts off with a single 10 × 10 arc min, 5 arc sec resolution, image centered on the observing region. This serves to place subsequent smaller images in a broader solar context. The large image is followed by a sequence of 5 × 5 arc min images at full resolution through each SXT filter. In this example there is no looping within the sequence. The sequence takes about 1.5 min per execution and is arranged to provide thin-filter images and optical images at uniform cadence at twice that rate. This enhances our ability to observe small white-light flares and low-level activity.

The image intervals, dt, include set-up and data transfer time as well as exposure time. Except for the thick beryllium filter the intervals are dominated by the time to transfer data to telemetry. The interval dt can either be held fixed, with the automatic exposure control permitted to operate only within this constraint, or allowed to increase in response to the automatic exposure software in the DP. Note that while this simple example concentrates on a single target, every numbered image in the sequence is independent and could image any one of the locations stored in the nine observing-region registers. Thus, it is feasible to continuously monitor the activity at several locations on the Sun in quiet mode.

There are 8 sequence tables stored in non-volatile memory in the DP, 4 each for partial frame (PFI) and full frame (FFI) images. At any given time 6 tables are designated for use under the 4 SOLAR-A science modes, QT/HIGH, QT/MED, FL/HIGH, and FL/MED. Sequence tables optimized for quiet-Sun or flare observations are sometimes quite different. Furthermore, the design of the cadence (number of loops) depends on the telemetry bit rate so the sequence table may be different between FL/HIGH mode (impulsive phase) and FL/MED mode (gradual phase) following the FL/HIGH mode. An 'entry table' is used to point to the desired sequence table for specific DP modes as shown in the following example:

Entry table

Data mode	TLM rate	Seq. table
QUIET (QT)	HIGH	FFI No. 1
QUIET (QT)	HIGH	PFI No. 1
QUIET (QT)	MED	FFI No. 2
QUIET (QT)	MED	PFI No. 2
FLARE (FL)	HIGH	PFI No. 3
FLARE (FL)	MED	PFI No. 4

For PFI observations in this example, No. 1 sequence table is used in the QT/HIGH mode. This will be automatically switched to sequence table No. 3 when FL/HIGH mode starts. (In this case, the sequence table No. 1 is optimized for QT/HIGH mode, and No. 3 for FL/HIGH mode.) If the bit rate is changed to MED in the gradual phase of the FL mode, the sequence table is switched to No. 4. The entry table numbers may be modified by real time or stored commands to achieve observing objectives. For instance, if we specify the sequence table No. 1 in the FL/HIGH column, then the same experiment sequence will continue regardless of the DP mode change to FL mode.

3.2.2. *Automatic Observing Region Selection*

The Automatic OR Selection (ARS) function utilizes patrol images taken for this purpose at regular intervals set by time commands or in response to a flare flag. There are two different ARS algorithms available when in the Quiet (QT) Mode and one algorithm while in the Flare (FL) Mode. Seach mode ARS is used to search the whole solar image for the four brightest sources in both QT and FL modes. Tracking mode ARS is used to track a feature as the region moves due to solar rotation, spacecraft pointing drift, or as the location of brightest emission evolves in QT mode. The QT ARS and FL ARS have separate parameters available to set up the exposure characteristics. The FL ARS has available its own automatic exposure control to help deal with the inordinate variation in X-ray brightness of flares. The accuracy of ARS source location is normally one patrol image pixel or 10 arc sec.

A patrol image is 42 × 21 arc min in size with a 10 arc sec (4 × 4 pixel) resolution. The area of the Sun covered in the search is therefore equivalent to the area labelled 'Full Frame Image' in Figure 12. As can be seen by comparison to the SMM flare locations plotted there, this adequately encompasses the active latitudes of the Sun.

The patrol image has highest priority and will interrupt acquisition of FFI or PFIs. The taking of patrol images is set in absolute time with an interval of 16 s to over an hour. Thus, by setting the time interval very long it is possible to prevent the taking of patrol images from interrupting, say, a movie sequence. QT and FL patrol images have independent cadences. It is possible to inhibit both patrol images and the ARS function.

There are nine observing region (OR) target registers in the DP to specify the locations of SXT observing regions. Five of these are filled by the ARS function and four by ground command. If ARS is inhibited, all nine registers may be loaded by ground command. Each register contains the location of the OR on the CCD and the number and shape of the mosaic of PFIs comprising an observing region.

The ninth OR register is redundantly filled with the location of the brightest feature by QT mode ARS to serve as the starting point for a flare search in response to a flare flag. The CCD exposure in process is aborted, a patrol image is taken and the FL ARS is activated at the time of the flare flag. The object is to center the flare observing region on the brightest feature as early as possible. If the flare is in the same observing region as was stored in the ninth OR register, flare observations will commence within 4 s. For an arbitray flare location the repositioning of the OR may require up to 6 s. The OR revised flare location is finally stored in the flare OR register.

Observing region (OR) table

OR No.	Location updated by
0	Quiet mode ARS
1	Quiet mode ARS
2	Quiet mode ARS
3	Quiet mode ARS
4	Quiet mode ARS
4	ART
5	ART
6	ART
7	ART
8	Flare mode ARS

3.2.3. *Automatic Observing Region Tracking*

While ARS will be useful to track bright X-ray structures on the Sun, sometimes it is necessary to keep the OR centered on a location, e.g., a coronal hole or emerging active region, that is not the brightest X-ray feature in the neighborhood. The Automatic OR Tracking (ART) software provides this function by tracking the movements of observing regions due to spacecraft attitude drift. Instead of changing the pointing of the telescope, the same function is served by choosing a diferent part of the CCD image. ART software uses the fine Sun sensor data of the SOLAR-A attitude control system for this purpose. At high data rate the correction is applied every 32 s. ART only works on the ground-commanded OR locations, not those selected by ARS – unless the contents of those registers are manually transferred to the four non-ARS registers.

3.2.4. *Automatic Exposure Control*

Because of the tremendous range in the X-ray brightness (e.g., Table III) of solar phenomena and the rapid change in X-ray intensity during flares it has been necessary to incorporate an Automatic Exposure Control (AEC) function in the SXT software. Every numbered image in a sequence table (Section 3.2.1) has its own AEC. This is implemented as follows. As a given image is read out from its image buffer to telemetry the number of pixels with intensity above an upper and the number below a lower threshold are counted and recorded. If the number of overbright pixels exceeds the table value (typically 10 pixels) the exposure is decreased or, if that is not possible, a thicker filter is selected. If the over-exposure test is passed, then the number of underbright pixels is compared to the table value (typically 100). If under-exposure is indicated, i.e., there are more pixels below the lower threshold than allowed, the exposure is increased or a thinner filter is selected for the next execution of that sequence table entry.

The AEC software runs in the DP which is a very busy real-time computer. However, the AEC algorithm is very fast so it takes only 6 s to update the exposure from the time the exposure was made. Since the AEC is a feed-back system with time delay, to assure stability of the AEC loop it is necessary that there be enough intervening images in the

sequence table to allow exposure adjustment before the same sequence table entry is again commanded. If necessary, say for a high cadence movie in which only a single kind of picture was desired, this can be accomplished by simply duplicating the desired parameters in at most 3 sequence table positions and setting the rest of the table positions to 'No operation'.

The AEC only works on partial frame images (PFI) or observing regions comprised of PFIs. The actual implementation of the AEC is more complicated than this simple description implies. The logic tree for achieving proper exposure under the formidable range of observing conditions experienced by the SXT is quite complex.

3.3. Image Cadence

The time resolution of the SXT depends in a complex way upon many different factors, some determined by the experiment itself and some dictated by things such as the time since a downlink contact and the occurrence of flares. SOLAR-A science operation utilizes two SXT control and telemetry modes. In the quiet (QT) mode 62.5% of available telemetry is devoted to SXT images because the Hard X-ray Telescope does not produce science data (cf. Ogawara *et al.*, 1991). In flare (FL) mode, SXT uses 50% of the telemetry. In QT mode interleaved full frame and partial frame images of up to eight different observing regions may be acquired. In FL mode FFI are not taken. In either mode images are acquired at a cadence determined by the rate of transfer of the data to telemetry. SXT housekeeping and status data are telemetered regularly in addition to the image data. These status data contain image header information such as filter combination and exposure time which are telemetered in synchronism with the image data.

In normal QT mode both FFI and PFI are acquired, with periodic interruption by patrol images. The priority order for image acquisition is (1) patrol, (2) FFI, and (3) PFI. This normally results in gaps in PFI cadence as schematically illustrated in Figure 13. Note that a patrol image is automatically taken at the time of switch to FL mode. If there is a high scientific priority for obtaining PFI movies with no gaps, the control structure of SXT makes this possible at the sacrifice of FFI and the taking of patrol images. It is also possible to structure the SXT sequence control tables to continue the QT PFI cadence on into the FL mode in order to provide unchanged monitoring of a specific region.

A switch from QT to FL mode can occur because of a flare flag or by command. The transition from FL to QT mode normally occurs because energetic flare emission has dropped below preset thresholds and preset time intervals have expired. See Ogaware *et al.* (1991) for a description of use of the flare flag and the SOLAR-A bubble data recorder to store and sometimes overwrite less important data in response to flares.

3.3.1. *Quiet Mode*

In quiet (QT) mode SXT always acquires both full frame (FFI) and partial frame (PFI) images. The cadence of exposures is strictly determined by telemetry transfer time unless the exposure and set-up time exceed this, in which case a dummy image is transmitted.

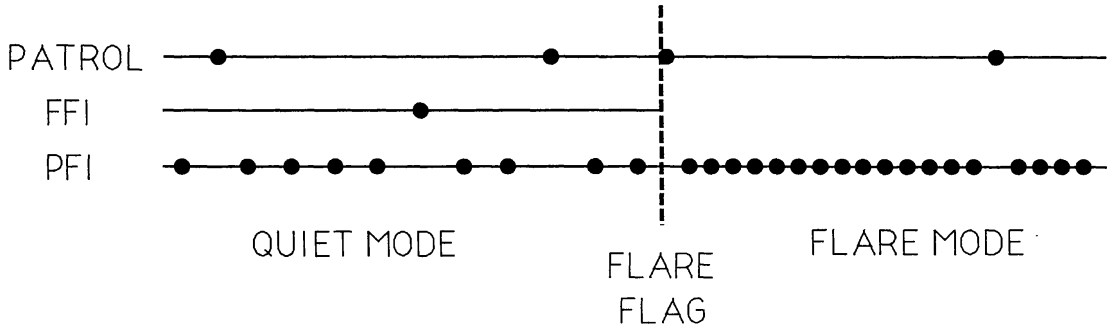

Fig. 13. Scheme of interleaving the 3 different types of SXT exposures. Each filled circle represents a CCD exposure. Time runs from right to left. This is only a schematic example, the relative frequency of the different types of exposures is subject to control over a wide range.

There are two telemetry modes. In the PFI dominant mode, PFI data are transferred with telemetry rate 4 times faster than that of FFI, while in the FFI dominant mode, *vice versa*. This effect is evident in the times tabulated in Table V. The observing sequence example given in Table IV corresponds to the case of PFI dominant mode and telemetry rate high.

Separate image registers or buffers are used within the DP to receive pictures from the CCD camera and pass the desired portions on to telemetry. Although FFI and PFI may use either buffer *A* or *B*, it is not possible to combine the telemetry allocated to *A* and *B* to achieve yet higher time resolution, nor is it possible to devote both buffers simultaneously to only FFI or PFI.

For the fastest PFI cadence of 2 s image^{-1} the maximum allowable exposure duration is approximately 0.5 s in order to provide time to read out the CCD image and position the filter wheels. Table V provides a summary of information on SXT pixel size, image size, time resolution and maximum exposure times for basic full frame and partial frame images. Note that the very long maximum exposure times given for full frame images, while formally correct, are not generally desirable because of image smearing from pointing drift and waste of telemetry, i.e., no PFI can be taken during the long FFI exposure. Only very faint features such as the interior of coronal holes will require exposures greater than 10 or 20 s.

3.3.2. *Flare (FL) Mode*

In flare (FL) mode SOLAR-A assigns 12.5% of telemetry (which in QT mode is available to SXT) to the Hard X-ray Telescope and commands high telemetry rate for a predefined time interval. As illustrated in Figure 13, the taking of FFI is stopped, although the current contents of the FFI image buffer will eventually be transferred to telemetry and are not lost. In FL mode the interval between SXT images will be determined by the number of PFI in the observing region. For a single PFI the image cadence is 2 s at high telemetry rate and 16 s at medium rate.

1991SoPh..136...37T

TABLE IV

SXT sequence table structure

Basic sequence table

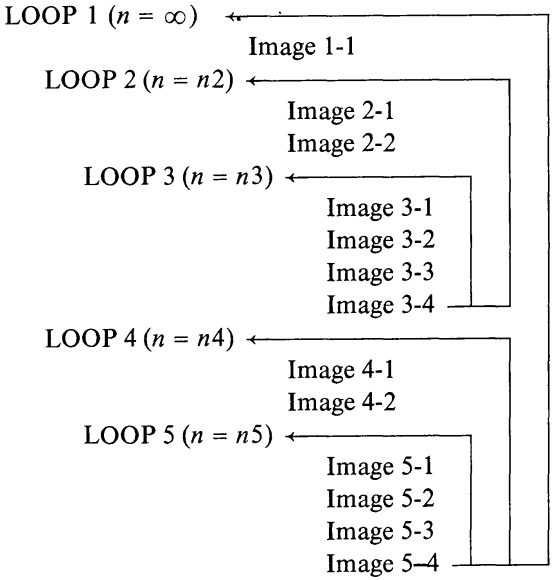

PFI sequence table (example)

	Filter	Pixel sum	Obs. region	dt (s)
Image 1-1	Al 1265 Å	2 × 2	2 × 2	8
($n2$ = 1)				
Image 2-1	4308 Å	1 × 1	2 × 2	8
Image 2-2	4600 Å	1 × 1	2 × 2	8
($n3$ = 1)				
Image 3-1	Al/Mg/Mn	1 × 1	2 × 2	8
Image 3-2	Mg 2.52 μm	1 × 1	2 × 2	8
Image 3-3	Al 11.6 μm	1 × 1	2 × 2	8
Image 3-4	Al 1265 Å	1 × 1	2 × 2	8
($n4$ = 1)				
Image 4-1	4308 Å	1 × 1	2 × 2	8
Image 4-2	4600 Å	1 × 1	2 × 2	8
($n5$ = 1)				
Image 5-1	Be 119 μm	1 × 1	2 × 2	16
Image 5-2	Open	1 × 1	2 × 2	8
Image 5-3	NOP			0
Image 5-4	NOP			0
			Total sequence time = 96 s	

NOP = no operation = skip.

TABLE V

SXT image size, time resolution and exposure time

Telemetry		On-CCD sum	Pixel (arc sec)	Partial frame image		
Rate	Mode			Image size (arc min)	Time resol. (s)	Max. expos. (s)
High	PFI dom.	1 × 1	2.45	2.6 × 2.6	2.0	0.5
		2 × 2	4.91	5.2 × 5.2	2.0	0.5
		4 × 4	9.81	10.5 × 10.5	2.0	0.5
High	FFI dom.	1 × 1	2.45	2.6 × 2.6	8.0	6.5
		2 × 2	4.91	5.2 × 5.2	8.0	6.5
		4 × 4	9.81	10.5 × 10.5	8.0	6.5
Med	PFI dom.	1 × 1	2.45	2.6 × 2.6	16.0	14.5
		2 × 2	4.91	5.2 × 5.2	16.0	14.5
		4 × 4	9.81	10.5 × 10.5	16.0	14.5
Med	FFI dom.	1 × 1	2.45	2.6 × 2.6	64.0	62.5
		2 × 2	4.91	5.2 × 5.2	64.0	62.5
		4 × 4	9.81	10.5 × 10.5	64.0	62.5

Telemetry		On-CCD sum	Pixel (arc sec)	Full frame image		
Rate	Mode			Image size (arc min)	Time resol. (min)	Max. expos. (s)
High	FFI dom.	1 × 1	2.45	41.9 × 20.9	4.27	254.5
		2 × 2	4.91	41.9 × 41.9	2.13	126.5
		4 × 4	9.81	41.9 × 41.9	0.53	30.5
High	PFI dom.	1 × 1	2.45	41.9 × 20.9	17.07	1022.5
		2 × 2	4.91	41.9 × 41.9	8.53	510.5
		4 × 4	9.81	41.9 × 41.9	2.13	126.5
Med	FFI dom.	1 × 1	2.45	41.9 × 20.9	34.13	2046.5
		2 × 2	4.91	41.9 × 41.9	17.07	1022.5
		4 × 4	9.81	41.9 × 41.9	4.27	254.5
Med	PFI dom.	1 × 1	2.45	41.9 × 20.9	136.53	8190.5
		2 × 2	4.91	41.9 × 41.9	68.27	4094.5
		4 × 4	9.81	41.9 × 41.9	17.07	1022.5

3.3.3. *SXT High Time-Resolution Mode*

It is possible that high-resolution pictures could reveal quite fast flare phenomena in soft X-rays. To permit investigation of this possibility a special high time-resolution mode has been implemented within the SXT. In this case a PFI is divided horizontally (E–W) into 2 or 4 sub-images, one of which is acquired at twice or four times the normal rate. Each sub-image is a separate exposure timed, and with its region of interest (ROI) selected, by logic in the SOLAR-A microprocessor. As these 16 or 32 line ROIs are transferred to the DP they are combined into what the DP thinks is a normal 64-line

PFI. The disassembly of the images into a high time resolution (0.5 or 1 s) movie of 16 × 64 or 32 × 64 pixel images is done on the ground.

In order to maintain the fast cadence of this the high time-resolution mode certain restrictions apply. Exposures must be short and filter alternation is not possible from one frame to the next. Only a single observing region can be used but the usual on-chip pixel summation is permitted. Automatic exposure control is allowed under the same considerations as for a normal PFI.

4. Conclusion

The opportunity to take scientific instruments beyond the atmosphere of the Earth has enabled scientists to gain new knowledge on a grand and beautiful scale. The X-ray telescopes of the Skylab missions in the decade of the 1970s provided humankind's first extended look at phenomenon in the hot, dynamic outer atmosphere of a star. With the SOLAR-A soft X-ray telescope, thanks to improved technology, we have the opportunity to advance beyond Skylab with a simpler, smaller and less costly instrument. As we have described in the previous sections, the SXT provides innovative features catering to a wide range of observing targets. Thanks to phenomenal advances in data processing technology the SXT images should be much more easily and quickly accessible to the human mind than the earlier observations. For the best use of such elaborations, we hope that the SXT as well as the SOLAR-A mission survives for longer than is nominally expected, since it may be possible to study the solar-cycle dependency of various coronal parameters with a degree of reliability not previously attained. For flare studies the combination of SXT and the other SOLAR-A instruments provide a scientific capability much greater than the sum of the parts. We consider ourselves very fortunate to be able to contribute to these investigations and are eager to begin the mission.

Acknowledgements

We are grateful to our Japanese and American colleagues whose initiative and enthusiasm are responsible for the opportunity to have the SXT collaboration for the SOLAR-A mission. We especially recognize the leadership of Dr H. Hudson and the late Prof. K. Tanaka. We owe special thanks to our many scientific and engineering colleagues who have contributed to the design, fabrication, and testing of SXT. Among them K. Nariai and T. Watanabe for X-ray optics; T. Cruz and W. Rosenberg for aspect optics; K. Appert and D. Kyrie for electronics; D. Akin for shutter design; D. Murray, B. Costanzo, T. Hasui, and A. Hagiwara for thermal design; J. Vieira and K. Gowen for mechanical design; R. Stern for the CCD; C. Feinstein, W. Brooker, and L. Shing for test and calibration, I. Kondo for control system architecture; T. Kato and A. Yamaguchi for supporting SXT testing at ISAS; D. T. Roethig for computer and e-mail support; B. Rix, M. Finch, F. Friedlaender, D. Kauffman, and W. Jaynes for contract and program management; R. Fielder, S. Taylor, and T. Iwata for secretarial support, and N. Nitta for quick-look software.

We acknowledge the enhusiastic contribution in building the SXT portion of the SOLAR-A data processor (DP) by the Fujitsu DP/SXT team (I. Odaki, T. Tanaka, M. Kurihara, K. Nomura, and M. Kojima) led by S. Kubo. M. Abe of Systems Engineering Consultants Co., Ltd., led by I. Akiyama, made major contributions to software development. We also thank NEC Corp., especially M. Matsui and Y. Masumoto, for the integration of SXT to the SOLAR-A spacecraft.

The SXT program in the U.S. has been wisely and collegially managed and administered by C. Pellerin and J. Lintott of NASA headquarters and R. Ise and H. Hill of NASA Marshall Space Flight Center. The SXT CCD camera was provided by the Jet Propulsion Laboratory and we owe special thanks to L. Hovland, T. Bursch, J. Janesick, J. Daniels, M. Schwockert, T. Radey, E. Villegas, A. Collins, and R. White. It is only thanks to the expertise and cooperation of J. Hynecek and I. Fujii of Texas instruments that SXT has an excellent CCD. We have enjoyed outstanding teamwork and technical performance from our SXT subcontractors:

– *X-ray mirror*: United Technology Optical Systems (A. Slomba, R. Kusha, G. Hull-Allen, M. Laughlin).

– *Carbon fiber metering tube*: Fiber Technology Corp. (B. Lundy).

– *Filter wheel and shutter motor*: Shaeffer Magnetics.

– *X-ray filters*: Luxel Corp. (G. Steele, F. Powell).

– *Optical filters*: Andover Corp., Perkin–Elmer.

The program has been supported at Lockheed under contract NAS8–37334 with NASA Marshall Space Flight Center and by the Lockheed Independent Research Program.

References

Acton, L., Morrison, M., Janesick, J., and Elliott, T.: 1991, *Proc. SPIE, Charge-Coupled Devices and Solid State Optical Sensors* **1447**, 123.

Bendinelli, O.: 1991, *Astrophys. J.* **366**, 599.

Bruner, M. E., Acton, L. W., Brown, W. A., Stern, R. A., Hirayama, Y., Tsuneta, S., Watanabe, T., and Ogawara, Y.: 1989, in J. H. Waite, J. L. Birch, and R. L. Moore (eds.), *Proceedings of the 1988 Yosemite Conference on Outstanding Problems in Solar System Plasma Physics: Theory and Instrumentation,* Am. Geophysical Union Monograph, Vol. 54, p. 187.

Craig, I. J. D. and Brown, J. C.: 1986, *Inverse Problems in Astronomy*, Adam Hilger Ltd., Bristol and Boston.

Fludra, A. and Sylwester, J.: 1986, *Solar Phys.* **105**, 323.

Hynecek, J.: 1979, *IEEE IEDM Tech. Dig.* **611**.

Janesick, J., Hynecek, J., and Blouke, M.: 1981, *Proc. SPIE, Solid-State Imagery for Astronomy* **290**, 165.

Janesick, J., Klaasen, K., and Elliott, T.: 1987, *Opt. Eng.* **26**, 972.

Kane, S. R., Anderson, K. A., Fenimore, E. E., Klebesadel, R. W., and Laros, J. G.: 1979, *Astrophys. J.* **233**, L151.

Lemen, J. R., Claflin, E. S., Brown, W. A., Bruner, M. E., Catura, R. C., and Morrison, M. D.: 1989, *Proc. SPIE, X-Ray/EUV Optics for Astronomy and Microscopy* **1160**, 316.

Lemen, J. R., Acton, L. W., Brown, W. A., Bruner, M. E., Catura, R. C., Strong, K. T., and Watanabe, T.: 1991, *Adv. Space Res.* (to be published).

McTiernen, J.: 1991, in R. Canfield and Y. Uchida (eds.), *Proceedings of K. Tanaka Memorial Symposium*, Springer-Verlag, Berlin (to be published).

Mewe, R., Gronenschild, E. H. B. M., and van den Oord, G. H. J.: 1985, *Astron. Astrophys. Suppl. Series* **62**, 197.

Mewe, R., Lemen, J. R., and van den Oord, G. H. J.: 1986, *Astron. Astrophys. Suppl. Series* **63**, 511.
Morrison, M. D., Lemen, J. R., Acton, L. W., Bentley, R. D., Kosugi, T., Tsuneta, S., Ogawara, Y., and Watanabe, T.: 1991, *Solar Phys.* **136**, 105 (this issue).
Nariai, K.: 1987, *Appl. Optics* **26**, 4428.
Nariai, K.: 1988, *Appl. Optics* **27**, 345.
Ogawara, Y., Takano, T., Kato, T., Kosugi, T., Tsuneta, S., Watanabe, T., Kondo, I., and Uchida, Y.: 1991, *Solar Phys.* **136**, 1 (this issue).
Sakurai, T.: 1990, in Y. Osaki and H. Shibahashi (eds.), *Progress of Seismology of the Sun and Stars*, Springer Lecture Notes in Physics, No. 367, p. 253.
Strong, K. T. and Lemen, J. T.: 1987, unpublished work.
Strong, K. T., Acton, L. W., Brown, W. A., Claflin, S. L., Lemen, J. R., and Tsuneta, S.: 1991, *Adv. Space Res.* (to be published).
Vaiana, G. S., Van Speybroek, L., Zombeck, M. V., Krieger, A. S., Silk, J. K., and Timothy, A.: 1977, *Space Sci. Instr.* **3**, 19.
Watanabe, T.: 1987, *Bull Tokyo Astron. Obs. 2nd Ser.* **277**, 3213.